2009

Modeling of Viscous Shock Tube Using ES-BGK Model Kinetic Equations

S Chigullapalli
Purdue University

A Venkattraman
Purdue University

Alina A. Alexeenko
Purdue University - Main Campus, alexeenk@purdue.edu

47th AIAA Aerospace Sciences Meeting Including The New Horizons Forum and Aerospace Exposition
5 - 8 January 2009, Orlando, Florida

AIAA 2009-1317

47th AIAA Aerospace Sciences Meeting, 5-8 January, 2009, Orlando, Florida

Modeling of Viscous Shock Tube Using ES-BGK Model Kinetic Equations

S. Chigullapalli*, A. Venkattraman*, and A.A. Alexeenko†
School of Aeronautics & Astronautics, Purdue University, West Lafayette, IN 47907

The viscous effects on unsteady shock wave propagation are investigated by numerical solution of the Boltzmann model kinetic equations. The kinetic equations are solved for two unsteady non-equilibrium flow problems, namely, the one-dimensional Riemann problem and a two-dimensional viscous shock-tube. The numerical method comprises the discrete velocity method in the velocity space and the finite volume discretization in physical space using various flux schemes. The discrete version of H-theorem is applied for analysis of accuracy of the numerical solution as well as of the onset of non-equilibrium. Simulations show that the maximum entropy generation rate in viscous shock tube occurs in the boundary layer / shock wave interaction region. The entropy generation rate is used to determine the time-variation of the speed of propagation of shock, contact discontinuity and rarefaction waves.

I. Introduction

Shock wave propagation in microscale geometries has been a subject of renewed interest recently due to challenges and opportunities arising with advances in microsystems. Many macroscale sensors and devices such as pumps, valves and engines have been implemented in mesoscale and microscale versions using the Micro-Electro-Mechanical Systems (MEMS) fabrication techniques for silicon and, more recently, metallic materials. To date, most of such microsystems involving a gas as the working fluid are based on low-speed flow phenomena. Exploitation of compressible flow mechanisms can potentially increase performance of microdevices. For example, micro wave rotor concept has been suggested[1] as a higher compression-efficiency alternative to spool microcompressors. Microscale pulsed detonation engine[2] has been recently demonstrated and may be used to provide power densities higher than the combustion-based microthrusters.Additionally, a break-down of chip-level vacuum packaging for MEMS components involves the propagation of an initial pressure discontinuity through a planar micron-sized enclosure. Such applications of unsteady, high-speed flows in microsystems requires improved understanding of supersonic flows at microscale.

The problem of shock wave propagation in low pressure gas is dynamically similar to that at microscales if the surface roughness effects are negligible. The low-pressure shock tubes have been investigated starting as early as 1950s. The early experiments on shock wave propagation in low-pressure gases have demonstrated several important aspects of such flows, i.e. shock speed attenuation that becomes more prominent as the pressure decreases. A model was proposed by Duff[3] to account for the lower shock strength achievable for a given diaphragm pressure. Duff's model assumes that the flow between the contact discontinuity and shock wave is isentropic and, thus, does not include viscous effects explicitly and predicts the shock strength that is independent of the size of the tube (or Knudsen number). Recently Brouillette[4] revisited the shock wave propagation in viscous regime and developed a quasi one-dimensional theory for the shock attenuation including the effects of friction. Based on this model, the speed of propagation of flow perturbations is scale dependent and can be slower than the isentropic speed of sound. Zeitoun *et al*[5] studied the shock wave propagation in low-pressure shock tubes based on kinetic and continuum approaches. The

*Graduate Student, Student Member.
†Assistant Professor, AIAA Member.

shock speed attenuation to a subsonic velocity has been observed in computations for one case of a low initial pressure ratio. This was not attributed clearly to the scale effects and raised a question whether the determination of shock position based on a fixed, 5 %, rise in density allows to determine the shock speed accurately.

The main goal of the present study is investigation of viscous effects on unsteady shock wave propagation in a planar micro shock-tube. The unsteady non-equilibrium flow is investigated by numerical solution of the Boltzmann model kinetic equations for the velocity distribution function. The numerical method comprises the discrete ordinate method in the velocity space and the finite volume discretization in physical space using various flux schemes. The discrete version of H-theorem is applied for analysis of accuracy of the numerical solution.[6] The time-variation of shock wave speed is calculated based on density and entropy generation fields for different Knudsen numbers and compared with the inviscid and viscous flow theories.

II. Boltzmann Model Kinetic Equations

One class of model equations which is widely used is the Bhatnagar-Gross-Krook (BGK) type equations[7,8] with relaxation-type collision term. These equations are easier to solve when compared to the original Boltzmann equation though the number of dimensions in the phase space remains the same as in the Boltzmann equation. They also satisfy the H-theorem (which states that the production of entropy is always positive) and gives a Maxwellian phase density at equilibrium.[9] The phase density $f(x, \vec{c}, t)$ is governed by the equation,

$$\frac{\partial f}{\partial t} + c_x \frac{\partial f}{\partial x} + c_y \frac{\partial f}{\partial y} = -\nu(f - f_G) \tag{1}$$

One of the collision relaxation models that is widely used is the ellipsoidal-statistical model (ES-BGK)[10] where f_G is an anisotropic Gaussian given by

$$f_G = \frac{\rho}{\sqrt{det(2\pi\mathbb{T})}}\, e^{\left[-\frac{1}{2}(\vec{c}-\vec{u})^T \mathbb{T}^{-1}(\vec{c}-\vec{u})\right]} \tag{2}$$

where,

$$\begin{aligned} \rho\mathbb{T} &= \frac{1}{Pr}\rho RTI + \left(1 - \frac{1}{Pr}\right)\rho\ominus \\ \rho\ominus &= <(\vec{c}-\vec{u}) \otimes (\vec{c}-\vec{u})f> \\ \rho RTI &= <(\vec{c}-\vec{u}) \otimes (\vec{c}-\vec{u})f_\gamma> \end{aligned}$$

with f_γ being a Gaussian of the form $a\exp(-\Gamma C^2 + \gamma_i C_i)$ and ν is the collision frequency given by

$$\nu = \frac{Pr \cdot p}{\mu}$$

It should be observed that the collision frequency, ν, involves the Prandtl number, Pr as a free parameter. This allows the ES collision model to reproduce transport coefficients, viscosity and thermal conductivity, corresponding to an arbitrary Prandtl number. The collision term of the BGK model can be obtained as a special case of the ES collision model by substituting $Pr = 1$. We indicate this collision term by $-\nu(f - f_\gamma)$.

III. Entropy Generation Rate

The second law of Thermodynamics postulates the existence of a state function called the entropy and describes its properties. However, the most fundamental expression for entropy is given by the Boltzmann relation from statistical mechanics

$$S = k \ln \Omega \tag{3}$$

where S is the entropy, k is the Boltzmann constant and Ω is the statistical multiplicity of the gas. This quantity represents the total number of ways in which the total energy of the system can be distributed.

In this paper, only the translational component of entropy is discussed since all our computations are for a monatomic gas, Argon.

The expression for translational entropy in terms of the velocity distribution function can be derived (Eq. (37)[11]) as

$$S_{tr} = k \int_{-\infty}^{\infty} f(\vec{c}) \left[1 - \ln \left(\frac{h^3 f(\vec{c})}{m^3} \right) \right] d\vec{c} \tag{4}$$

The entropy generation rate based on kinetic description in terms of the velocity distribution function can be obtained from the Boltzmann transport equation. The final expression[11] for the entropy generation rate based on kinetic theory is given by

$$\dot{S} = \frac{\partial S}{\partial t} + \nabla . \left(k \int_{-\infty}^{\infty} \vec{c} f(\vec{c}) \left[1 - ln \left(\frac{h^3 f(\vec{c})}{m^3} \right) \right] d\vec{c} \right) \tag{5}$$

Since the formulation of this parameter involves the utilization of only statistical mechanics and kinetic theory, there are no inherent mathematical limitations in its calculation. In this paper, Eq. (5) will be referred to as *Kinetic Theory* expression for entropy generation rate.

For small deviations from local equilibrium, the entropy generation rate can be calculated as a function of macro-parameters only. This will be referred to as *Gas Dynamic* expression[12,13] for entropy generation rate and is given by

$$\dot{S} = \frac{\Phi}{T} + \frac{\kappa}{T^2} (\nabla T . \nabla T) \tag{6}$$

where Φ is the viscous dissipation function and $\kappa = \mu C_p / Pr$

$$\begin{aligned} \dot{S} = \frac{2}{3} \frac{\mu}{T} \left[\left(\frac{\partial u}{\partial x} \right)^2 + \left(\frac{\partial v}{\partial y} \right)^2 + \left(\frac{\partial u}{\partial x} - \frac{\partial v}{\partial y} \right)^2 + \frac{3}{2} \left(\frac{\partial u}{\partial y} + \frac{\partial v}{\partial x} \right)^2 \right] \\ \frac{\kappa}{T^2} \left[\left(\frac{\partial T}{\partial x} \right)^2 + \left(\frac{\partial T}{\partial y} \right)^2 \right] \end{aligned} \tag{7}$$

The expression for the entropy generation rate based on kinetic theory was derived from the Boltzmann Transport Equation using the fact that the entropy generation rate is the variation of entropy due to collisions. In DSMC simulations, the variation due to collisions cannot be computed directly whereas in an approach based on model kinetic equations, the explicit form of the collision term facilitates this rate to be computed directly. The entropy generation rate calculated using the collision term is given by

$$\dot{S_{coll}} = -\nu \int_{-\infty}^{\infty} (f(\vec{c}) - f_0(\vec{c})) ln \left(\frac{h^3 f(\vec{c})}{m^3} \right) d\vec{c} \tag{8}$$

with f_0 being an anisotropic Gaussian or a Gaussian, depending on the collision model. This term will be referred to as *Kinetic Theory - rhs* expression for entropy generation rate. It should be mentioned that this term will always be positive if the model kinetic equation considered satisfies the H-Theorem.

IV. Numerical Modeling Approach

There have been various attempts in the past to apply different numerical schemes to obtain solutions to the model kinetic equations.[14] In general, the numerical method that is applied, should conserve mass, momentum and energy. It should also satisfy Boltzmann's H-Theorem and ensure positivity of the solution. Here, we present the numerical method in one spatial dimension and three dimensions in microscopic velocity. The governing kinetic equation in one-dimension is

$$\frac{\partial f}{\partial t} + c_x \frac{\partial f}{\partial x} + c_y \frac{\partial f}{\partial y} = -\nu (f - f_0) \tag{9}$$

For the numerical solution of the system it is convenient to non-dimensionalize the variables. Each dimensionless quantity is referred to its upstream values ($\rho_0 = \rho_1, T_0 = T_1$), the reference speed $u_0 = \sqrt{2RT_1}$

and the reference time $t_0 = \frac{L}{u_0}$. The reference value for the distribution function is n_0/c_0^3. Entropy is non-dimensionalized by $S_0 = \rho_1 R$ and entropy generation rate by $\rho_1 R u_0/L$.

The space variable is discretized on a Cartesian grid defined by nodes x_{i_x,i_y} and y_{i_x,i_y}. The microscopic velocities in the x, y, z directions, c_x, c_y, c_z, are discretized using a conventional discrete ordinate method with uniform velocity abscissas. In the current formulation, a discrete velocity $(c_x(j_1), c_y(j_2), c_z(j_3))$ of the grid is denoted by c_j , where $j = (j_1, j_2, j_3)$. Finally, we also choose a time discretization with $t = n\Delta t$.

Upon approximation of the model kinetic equation by a Finite Volume Scheme,

$$\frac{\partial f}{\partial t} = -\frac{1}{\Delta x}[F_{i_x+\frac{1}{2},i_y,j} - F_{i_x-\frac{1}{2},i_y,j}] - \frac{1}{\Delta y}[F_{i_x,i_y+\frac{1}{2},j} - F_{i_x,i_y-\frac{1}{2},j}] - \Delta t \nu_i (f_{i_x,i_y,j} - f_{0_{i_x,i_y,j}}) \tag{10}$$

where $F_{i_x+1/2,i_y}$ and $F_{i_x-1/2,i_y}$ refer to the flux at the left and right faces of a cell. And $F_{i_x,i_y+1/2}$ and $F_{i_x,i_y-1/2}$ refer to the flux at the top and bottom faces of a cell.

IV.A. Spatial Fluxes

The first and second-order schemes used are as described by Mieussens *et.al.*[14] The third-order fluxes were computed using the Weighted Essentially Non-Oscillatory(WENO) schemes described by Zhou *et.al.*[15]

IV.B. Time Integration

In order to ensure high-order accuracy in time integration, we use second and third-order Total Variation Diminishing (TVD) Runge-Kutta schemes described by Zhou *et.al.*[15]

IV.C. Calculation of Entropy Generation Rate

The H-theorem states that the entropy generation rate, given by Eq. (6), is a strictly positive function. Due to numerical errors in space, time and velocity discretization, the discrete solution of Eq. (9), in general, may not satisfy the discrete version of H-theorem. This is due to the fact that the discretized form of the moment transfer equation for entropy may not be satisfied for a distribution function which is obtained as a discrete solution of Eq. (9). The requirement that for a discrete solution of Eq. (9), the entropy generation rates calculated using discrete versions of Eq. (5) and Eq. (8)are equal in magnitude, upto a certain precision, can be used as a criteria for accuracy of numerical simulations.

In discretized form, Eq. (5) can be written as:

$$\dot{S}_i = L^t(S_i) + L^x\left(\sum_j c_j f_{i,j}\left[1 - ln\left(\frac{h^3 f_{i,j}}{m^3}\right)\right]\Delta c_j\right) \tag{11}$$

where L^t is the operator for a second-order central difference scheme and L^x is a third order approximation of fluxes for the first derivative. The entropy generation rate for the collision term can be calculated using the discretized form of Eq. (8) given by

$$\dot{S}_{coll_i} = -\nu \sum_j (f_{i,j} - f_{0_{i,j}}) ln\left(\frac{h^3 f_{i,j}}{m^3}\right)\Delta c_j \tag{12}$$

The discrete velocity models for equation Eq. (9) have been formulated[14,16,17] such that the positivity of the entropy generation rate due to collisional relaxation, Eq. (12), is strictly enforced. However, numerical discretization errors may lead to significant deviation between the transport, Eq. (5), and collisional, Eq. (12), expressions for entropy generation rate.

Below we present calculations of entropy generation rates for shock tube problems using various numerical schemes. The calculation of entropy generation rate is not computationally intensive and can be easily incorporated in the numerical procedure. As will be shown below the discretized version of H-theorem can be used as a convenient and powerful indicator of the accuracy of the numerical solution as well as of the onset of non-equilibrium.

V. Results and Discussion

The model kinetic equations are applied to two different problems. The first problem considered is an unsteady Riemann problem of that of a one-dimensional shock tube. The second is a two-dimensional viscous shock tube involving regions of non-equilibrium. First and second-order accurate fluxes are obtained using the minmod flux limiter. To compute the third order fluxes, we use the Weighted Essentially Non-Oscillatory (WENO) scheme. For the unsteady problem, second-order and third-order TVD Runge Kutta schemes were used for time marching. All the numerical schemes were implemented in FORTRAN 90 and the parallel version of the code was implemented using MPI libraries.

V.A. 1D Riemann Problem

A well-known one-dimensional flow problem is the Riemann problem,[18] which treats the development of a flow due to an initial discontinuity. Removing the diaphragm separating the gas in the two reservoirs, results in a characteristic wave system consisting, in general, of three waves, a shock wave, an expansion fan, and a contact discontinuity. The inviscid shock-tube problem can be solved exactly using gas-dynamic theory. Riemann problem is depicted in Fig.1.

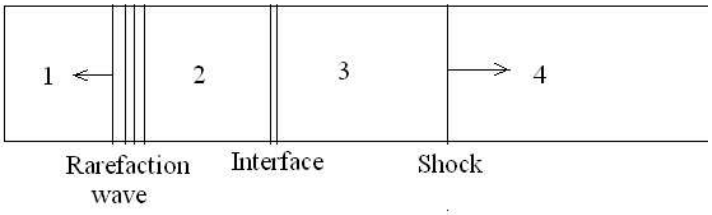

Figure 1. Shock Tube

We assume that the diaphragm in the shock tube is located at $x = L/2$ where L is the length of the domain. Argon gas to the left of the interface is at a pressure of 10 Pa and temperature $300K$. This corresponds to a density of 1.603×10^{-4} kg/m^3. The pressure on the right side of the interface is set to 1 Pa and temperature is set to $300K$. In the non-dimensional form, these values are shown in Table 1. For the computations shown, the number of cells in the physical space for a grid converged solution is 1000. The velocity space was discretized using a $20 \times 20 \times 10$ grid. The entropy generation rate corresponding to the Riemann Problem includes the unsteady component and is calculated using Eq.(5).

Table 1. 1D Shock-tube: Initial conditions to the left and right of interface.

Property	Left Zone	Right Zone
Density	1.0	0.1
x-velocity	0	0
Temperature	1.0	1.0
Pressure	1.0	0.1

From Fig. 2 it can be seen that the profiles for macro-parameters for the different flux schemes agree well. The solutions from first-order and second-order schemes differ by less than 1% and 0.1% from the third-order schemes respectively but they show regions of non-positive entropy generation rate as shown in Fig. 3. However, the entropy generation rate profile for solution obtained using the third-order WENO scheme agrees well with the gas dynamic expression and also with the entropy generation rate obtained using the collision term as shown in Fig. 4. Clearly, solution in Fig. 3 is not a grid converged solution whereas it is in Fig. 4. Thus entropy generation rate can be an indicator of grid convergence of numerical solution. The three peaks in the entropy generation rate profile from right to left correspond to the location of shock, contact discontinuity and rarefaction fan respectively. Their locations and velocities can then be calculated by tracking these peaks over time.

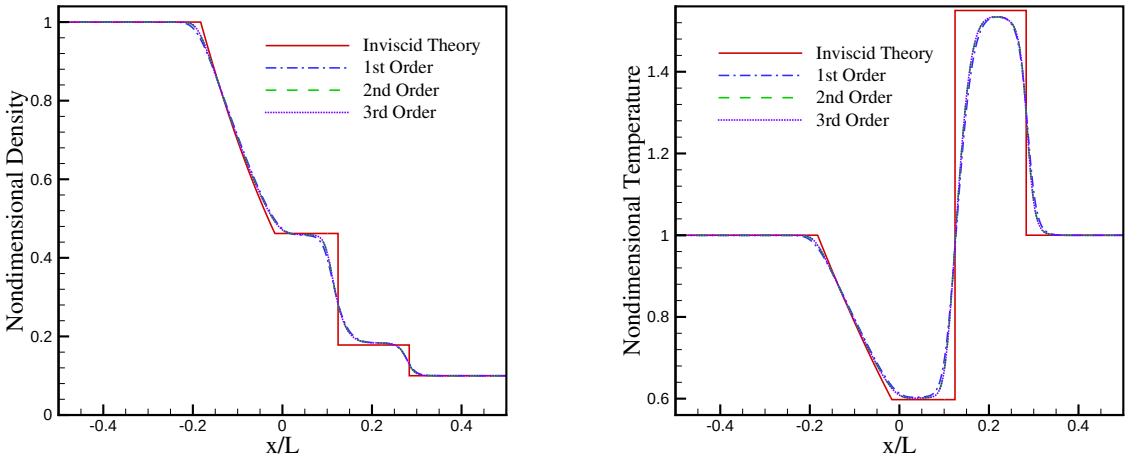

(a) Density (b) Temperature

Figure 2. Comparison of density and temperature profiles at non-dimensional time $t = 0.2$ for different flux schemes using 1000 cells.

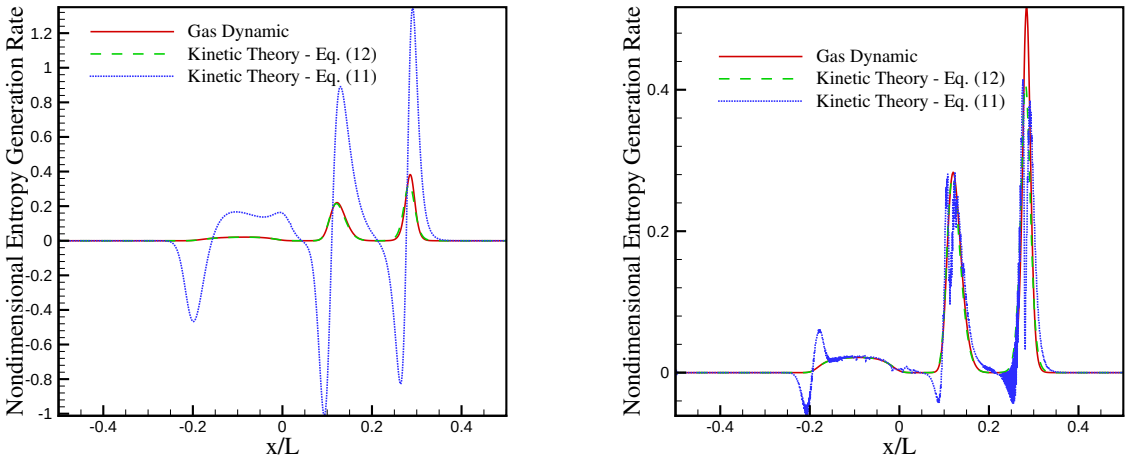

(a) First Order Flux Scheme (b) Second Order Flux Scheme

Figure 3. Comparison of entropy generation rates at non-dimensional time $t = 0.2$ for first and second order flux schemes using 1000 cells.

V.B. 2D Shock-Tube Problem

In commonly used shock-tubes in laboratories, the boundary layer effects are negligible and the problem can be considered one-dimensional for all practical purposes making it similar to a one-dimensional Riemann problem described in the previous subsection. However, to get high Mach numbers, the initial pressure ratio is extremely high and this increases the burden on vacuum pumps. In case a desktop shock tube were used, it is easier and faster to pump down the chambers to get the high pressure ratios due to their smaller dimensions. But as the size of the shock tube is reduced, the boundary layer effects are not negligible.[1] Shock tubes are also used to induce faster combustion and their use in micro devices is an active area of research.[4,5] Here, we consider a two-dimensional flow in a shock tube and present results for the simulation of two cases, with Knudsen numbers (Kn) in the range 0.01-1, using the kinetic model equations and compare the lower Knudsen number case with compressible Navier-Stokes simulations.

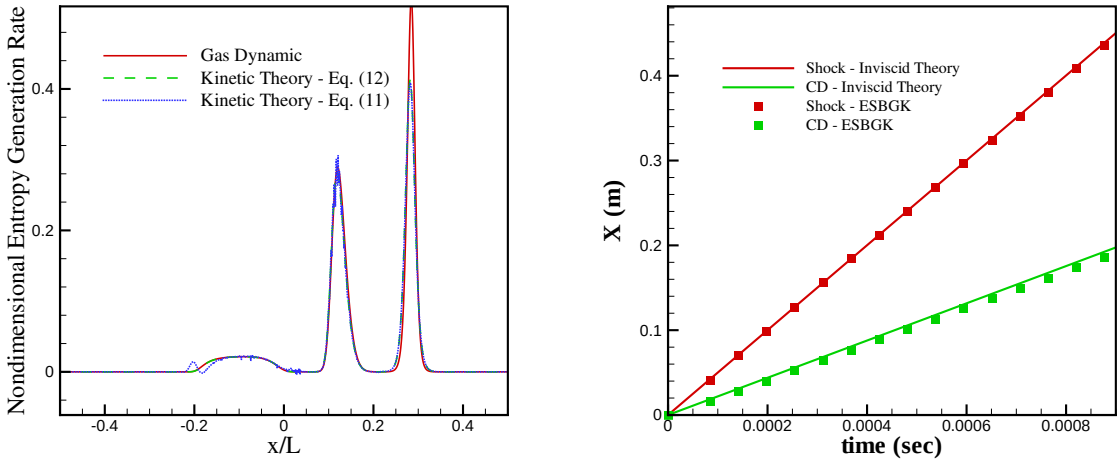

(a) Third Order Flux Scheme

(b) Shock/CD locations

Figure 4. a)Entropy generation rate at non-dimensional time $t = 0.2$ for third order WENO scheme using 1000 cells. b)Shock/CD locations calculated from peaks in entropy generation rate.

The length and height of the channel were chosen to be 1 m and 0.05 m respectively. This gives Knudsen numbers of 0.01 and 0.1 in the high and low pressure sections respectively. For ease of computation, only the top half of the domain has been used. This implies, the top boundary is a wall maintained at a constant temperature of $T = 300$K and the bottom is a symmetry boundary. The initialization is same as in the 1D Riemann problem. The dimension of the phase space in the Kinetic WENO solver is taken to be $320 \times 24 \times 20 \times 20 \times 10$ with a successive ratio of 1.1 in the y-direction. For the compressible Navier-Stokes simulation, a 300×100 mesh was used with a non-uniform grid in the y-direction with a with a local stretching factor (lsf) of 0.1 where lsf is $\Delta y_{i+1}/\Delta y_i - 1$. Figures 5 show the velocity and pressure contours for both Navier-Stokes and WENO kinetic solutions at time $t^* = 2.12$ where $t^* = 1$ implies the theoretical time it takes for a shock to move a distance equal to h. It can be seen that the shock is more attenuated in the Navier-Stokes solution than in the WENO Kinetic solution. This is due to the slip effects that are accounted for in the kinetic equation but not in the Navier-Stokes simulation.

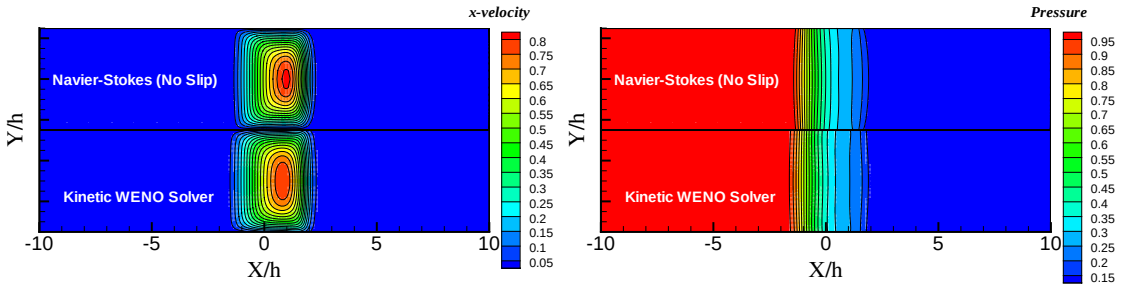

Figure 5. 2D shock-tube: x-velocity and pressure contours for $Kn = 0.01 - 0.1$ at $t^* = 2.12$.

V.B.1. Entropy and Entropy Generation Rate Fields

Figures. 6(a) and (b) show the map of x-velocity and entropy for four different times. As time increases, the zone of non-equilibrium expands and its extent can be found from the entropy generation rate profiles. At the axis of symmetry, the contours of entropy generation rate show three peaks corresponding to three different regions of non-equilibrium, the compression wave, the contact discontinuity, and the rarefaction wave. At the walls of the shock tube, the interactions between the boundary layer and the wave system, lead to a more complicated interaction giving only one peak in the entropy generation rate. Also, Fig. 7 shows that the maximum entropy generation rate in an unsteady shock tube occurs in the boundary layer and shock wave interaction region

The entropy and entropy generation rate fields are shown for four different timesteps 250,500,1000,1500 which correspond to $t^* = 1.06, 2.12, 4.24, 6.37$ respectively.

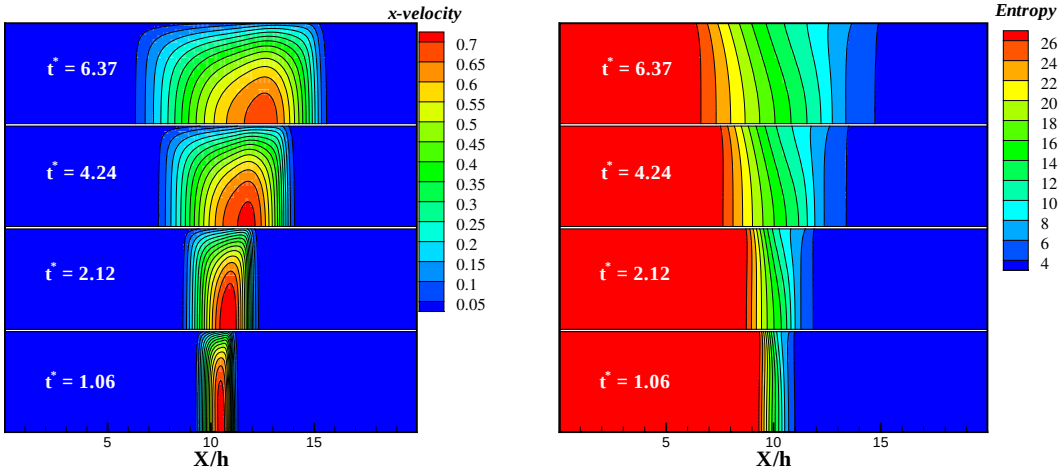

(a) Nondimensional x-velocity (b) Nondimensional Entropy

Figure 6. X-velocity and Entropy fields at 4 different instants of time.

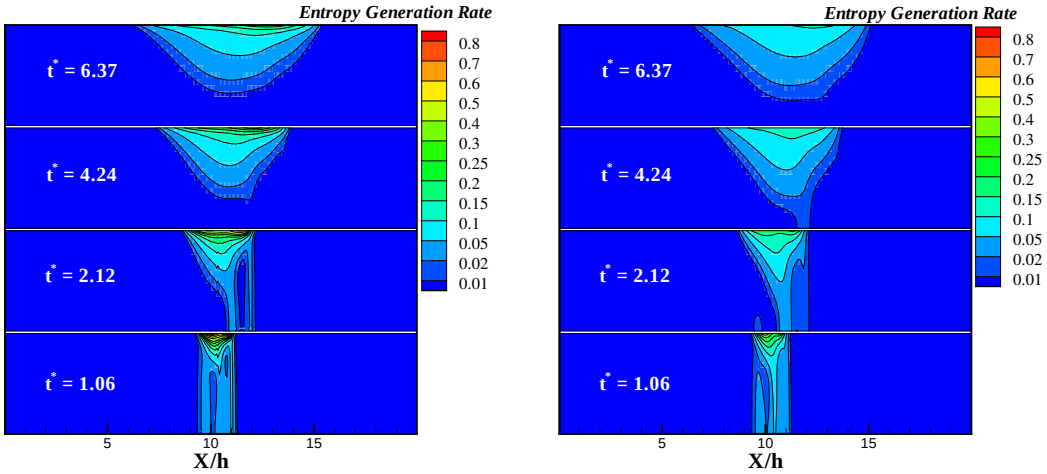

(a) Gas Dynamic Definition (b) Kinetic Theory - Eq. (12)

Figure 7. Entropy generation rate fields at 4 different instants of time for Knudsen 0.01 - 0.1.

V.B.2. *Shock/Contact Discontinuity Speed Attenuation*

In 1959, Duff through shock tube experiments at low initial pressures observed a decrease in shock velocity for a given pressure ratio. He proposed a simple model combining expressions for pressure jump across a shock, pressure decrease through steady expansion between shock and contact discontinuity and unsteady expansion in driver gas giving:

$$\left.\frac{P_1}{P_4}\right|_{Duff} = \left\{1 + \frac{M_s^2 + \beta_4 - 1}{(\beta_4 - 1)[M_s^2(\beta_4 + 1) - 1]}\right\}^{\frac{(\beta_4+1)}{2}} . \left.\frac{P_1}{P_4}\right|_{ideal} \tag{13}$$

where $\beta_4 = (\gamma_4 + 1)/(\gamma_4 - 1)$. Duff's model predicts a shock Mach number of 1.44 for a pressure ratio of 10 between the driver and driven gas. The Mach number from inviscid theory for the given pressure ratio is 1.55.

The locations of shock wave and contact discontinuity (CD) on the center-line were calculated by obtaining the location of the peaks in the entropy generation rate at the center-line and also at the edge from two different definitions, gas dynamic and kinetic theory-rhs, Eq. (12). Figures 9 show that the velocity of shock decreases as time progresses and should reach the velocity of the contact discontinuity eventually. Here, the domain wasn't large enough to capture this effect. The contact discontinuity starts off with a velocity higher than predicted by inviscid theory and then drops below that as time goes on. At the wall, there was only one peak in the entropy generation rate curve along the x-axis. This is due to the shock wave attenuation on interaction with the boundary layer. This peak starts with a velocity greater then the interface velocity but less than the shock velocity and eventually decreases to value way lower than that of the interface. The velocity of shock wave predicted using the collision term shows a linear profile as compared to a parabolic curve predicted by the gas dynamic expression.

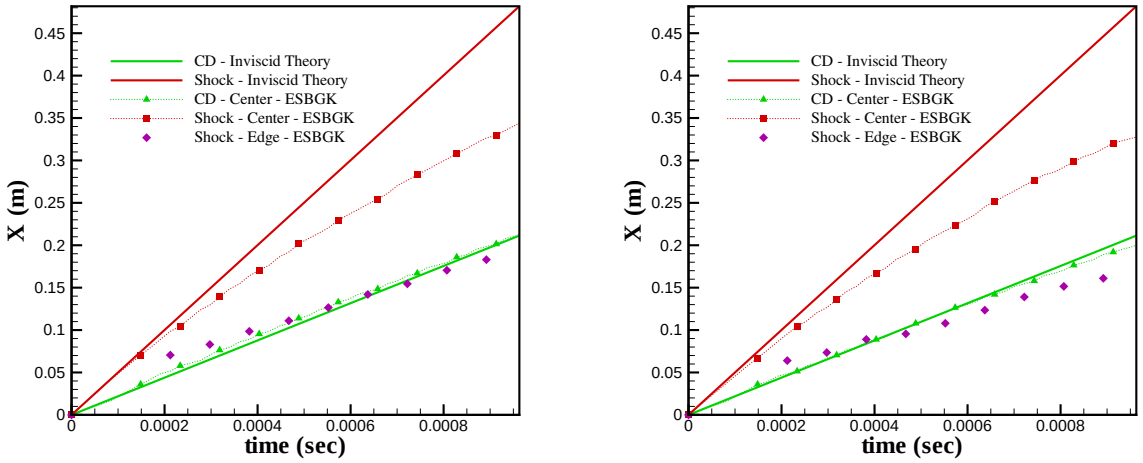

(a) Gas Dynamic Definition

(b) Kinetic Theory - Eq. (12)

Figure 8. Comparison of locations of shock and contact discontinuity vs time with the inviscid theory.

V.B.3. *Effects of Knudsen number*

A second case was run with the same grid resolution and pressure ratio but at a lower pressure as shown in Table 2. The Knudsen number in the left zone is 0.1 and in the right zone is 1.0. Case 2 gives profiles very different from Case 1 that are the manifestation of rarefaction effects. Figure 10 shows the static temperature and x-velocity profiles from the kinetic solver for both these cases at time $t^* = 6.37$. It can be seen from these profiles that the shock wave is slowed down more in Case 2 than in Case 1 when compared to the theoretical position of $x = 6.37h$ based on inviscid theory.[18]

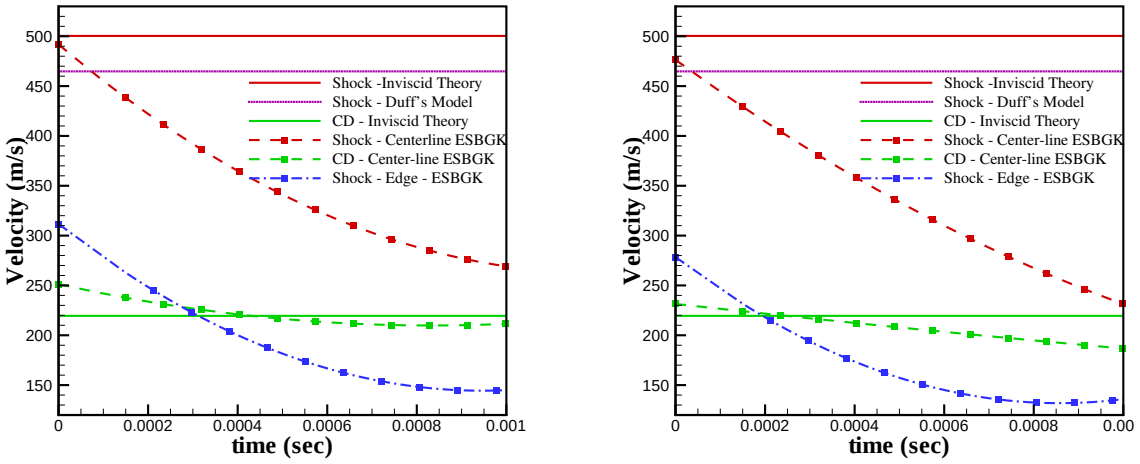

(a) Gas Dynamic Definition

(b) Kinetic Theory - rhs

Figure 9. Comparison of shock and contact discontinuity speeds with the inviscid theory and Duff's model.

Table 2. Initial conditions for the different cases

Property	Case 1	Case 2
ρ_0	$1.604E-4\text{kg}/m^3$	$1.604E-5\ \text{kg}/m^3$
T_0	300K	300K
P_0	10Pa	1Pa

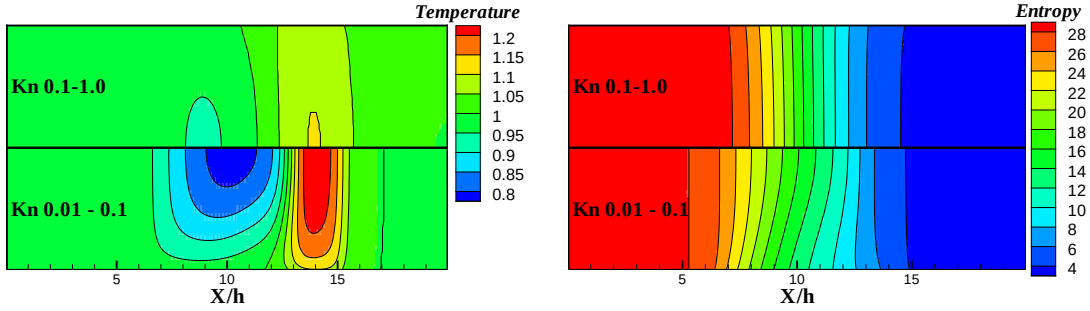

Figure 10. 2D shock-tube: Static temperature and entropy profiles for $Kn = 0.01 - 0.1$ and $Kn = 0.1 - 1.0$ at $t^* = 6.37$.

VI. Conclusions

The viscous effects on unsteady shock wave propagation in a 2D shock-tube are investigated by numerical solution of the Boltzmann model kinetic equations. The discrete version of H-theorem is applied for analysis of accuracy of the numerical solution as well as of the onset of non-equilibrium. Simulations show that the maximum entropy generation rate in viscous shock tube occurs in the boundary layer / shock wave interaction region and thus the flow between the contact dicontinuity and shock wave is highly non-isentropic contrary to the assumptions in Duff's model. The time-variation of shock speed is determined based on density and entropy generation fields. The shock speed attenuation increases significantly with the Knudsen number and, for high Knudsen numbers and low initial pressure ratio, decreases below the usual isentropic speed of sound.

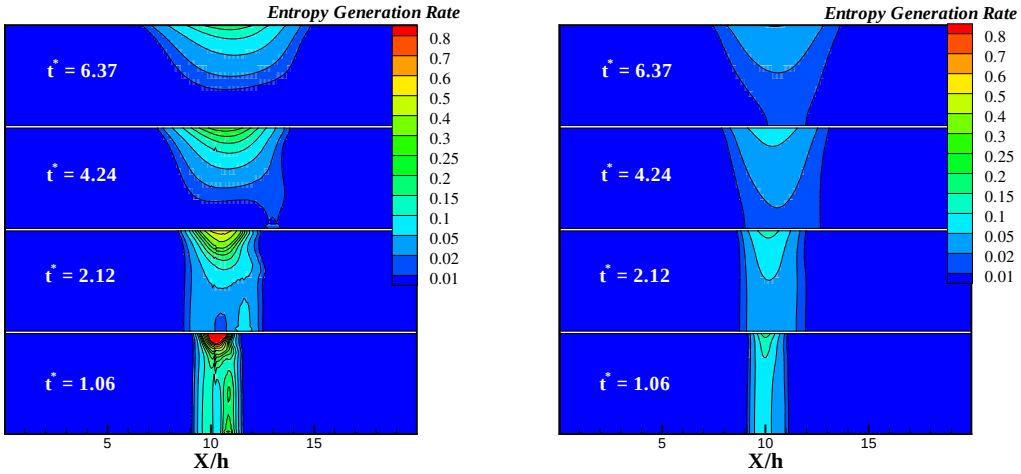

(a) Gas Dynamic Definition

(b) Kinetic Theory - rhs

Figure 11. Entropy generation rate fields at 4 different instants of time for Knudsen 0.1 - 1.0.

References

[1]Iancu, F. and Muller, N., "Efficiency of Shock Wave Compression in a Microchannel," *Microfluid Nanofluid*, Vol. 2, 2006, pp. 50–63.

[2]Kitano, S., Kimura, Y., Sato, H., and Hayashi, A., "Micro-Size Pulse Detonation Engine Performance, AIAA Paper 2007-581," *45th AIAA Aerospace Sciences Meeting and Exhibit, Reno, Nevada, Jan. 8-11, 2007*, AIAA.

[3]Duff, R. E., "Shock-tube performance at low initial pressure," *Physics of Fluids*, Vol. 2, 1959, pp. 207–216.

[4]Brouillette, M., "Shock Waves at Microscales," *Shock Waves*, Vol. 13, 2003, pp. 3–12.

[5]Zeitoun, D. E., Burtschell, Y., Graur, I. A., Ivanov, M. S., Kudryavtsev, A. N., and Bondar, Y. A., "Shock Waves at Microscales," *West-East High Speed Flow Field Conference*, Moscow, Russia, 2007.

[6]Chigullapalli, S., Venkattraman, A., Alexeenko, A. A., and Ivanov, M. S., "Non-Equilibrium Flow Modeling Using High-Order Schemes for the Boltzmann Model Equations," *40th Thermophysics Conference*, AIAA, Seattle,Washington, 2008.

[7]Bhatnagar, P. L., Gross, E. P., and Krook, M., "A model for collision processes in gases. I. Small amplitude processes in charged and neutral one component systems," *Physical Review*, Vol. 94, 1954, pp. 511.

[8]Krook, M., "Continuum equations in the dynamics of rarefied gases," *Journal of Fluid Mechanics*, Vol. 6, 1959, pp. 523.

[9]Andries, P., Tallec, P., J.Perlat, and Perthame, B., "The Gaussian-BGK model of Boltzmann equation with small Prandtl numbers," *European Journal of Mechanics.B/Fluids*, Vol. 19, 2000, pp. 83.

[10]Holway, L. H., "New statistical models for kinetic theory: Methods of construction," *Physics of Fluids*, Vol. 9, 1966, pp. 1658.

[11]Schrock, C. R., McMullan, R. J., and Camberos, J. A., "Continuum Onset Parameter Based on Entropy Gradients Using Boltzmann's H-Theorem," *43rd AIAA Aerospace Sciences Meeting and Exhibit*, AIAA, Reno, Nevada, 2005.

[12]Naterer, G. F. and Camberos, J. A., "Entropy and the Second Law Fluid Flow and Heat Transfer Simulation," *Journal of Thermophysics and Heat Transfer*, Vol. 17, No. 3, 2003, pp. 360–371.

[13]L.Boltzmann, *Lectures on Gas Theory*, Dover Publication, 1995.

[14]Mieussens, L. and Struchtrup, H., "Numerical comparison of Bhatnagar-Gross-Krook models with proper Prandtl number," *Physics of Fluids*, Vol. 16, No. 8, 2004, pp. 2797–2813.

[15]Zhou, T., Li, Y., and Shu, C.-W., "Numerical Comparison of WENO Finite Volume and Runge-Kutta Discontinuos Galerkin Methods," *Journal of Scientific Computing*, Vol. 16, No. 2, 2001, pp. 145–177.

[16]Mieussens, L. and Struchtrup, H., "Discrete-velocity models and numerical schemes for the Boltzmann-BGK equation in plane and axisymmetric geometries," *Journal of Computational Physics*, Vol. 162, No. 2, 2000, pp. 429–466.

[17]Frezzotti, A., "Numerical investigation of the strong evaporation of a polyatomic gas," *17th Symposium on Rarefied Gas Dynamics*, 1991.

[18]Schreier, S., *Compressible Flow*, Wiley, New York, 2nd ed., 1982.